Frequency Dynamics Constrained Unit Commitment With Battery Energy Storage

Yunfeng Wen, *Member, IEEE*, Wenyuan Li, *Fellow, IEEE*, Gang Huang, *Student Member, IEEE*, and Xuan Liu, *Member, IEEE*

***Abstract*—The decline of system inertia due to the increasing displacement of synchronous units by renewable units has introduced a major challenge on the frequency dynamics management of a power system. This paper discusses how fast-response battery energy storages can be used to maintain the frequency dynamic security. Immediately following a generation loss, the injections of batteries are adjusted instantly to ensure minimum power imbalance in the system. This control strategy is included in a novel formulation of the frequency dynamics constrained unit commitment, in which the impact of wind uncertainty is dealt with using interval-based optimization. The reformulation-linearization technique is applied to reformulate the original nonlinear model as a mixed-integer linear programming problem. Case studies on a six-bus system and the modified RTS-79 system demonstrate that the proposed method guarantees frequency security while still preserving economy without curtailing wind generation.**

***Index Terms*—Unit commitment, frequency, inertia, primary frequency control, battery energy storage, wind uncertainty.**

I. Introduction

FREQUENCY dynamics management is essential for the secure operation of a synchronous power system. The term "frequency dynamics" refers to the short-term transient period of frequency response following a sudden loss of generation. During this period, both the inherent system inertia and primary frequency response (PFR) are needed to arrest the frequency deviation across the interconnection.

Historically, it is not common for operators to manage the system inertia level in a large interconnection due to the plentiful inertia from conventional synchronous units (e.g., fossil fuel, hydro and nuclear) [1]. Current practices on defining primary reserve for PFR are based on simple capacity reserved requirements [2], i.e., setting the primary reserve amount of a generator at a certain percentage of its capacity. Generation scheduling and dispatch based on this simple approach is thus not sufficient to validate the frequency security during dynamic conditions.

With the increasing penetration of renewable generation in power systems, a considerable part of conventional synchronous units providing inertia response and PFR are being displaced by renewable units. However, wind and solar units typically provide low to zero inertia response because of their non-synchronous connection to a power system [3]. The increasing penetration of renewable generation thus reduces the total inertia of the system, and consequently poses a major challenge to the frequency dynamics management [4]. A report [5] on a U. K. system shows that, for 20 GW of load and 3.2 GW of wind power, the current capacity-based requirements for primary reserve definitions were incapable of meeting the frequency nadir limit. Electric power systems in Ireland [6], northwest of China [7] and Texas in USA [8] and especially some small isolated systems [1], [9] have experienced Rate-of-Change-of-Frequency (RoCoF) issues as a result of rapid expansion of wind generation.

Incorporating frequency related constraints in the Unit Commitment (UC) and Economic Dispatch (ED) could improve the frequency dynamics. Somuah and Schweppe [10] first reformulated the traditional ED by including an explicit constraint on the maximum system frequency deviation following a postulated disturbance. Restrepo and Galiana [11] formulated a PFR-constrained unit commitment that optimally schedules the reserve requirement for primary frequency regulation but only enforces a quasi-steady-state frequency limit. Ela *et al.* [12] designed an ancillary service market that explicitly incentivizing the provision of PFR. The scheduling, pricing and settlements needed for this market design were outlined. Extensive efforts [13]–[15] have been conducted to construct the frequency related constraints, such as the RoCoF and minimum frequency limits. The work presented in [15] established the sufficient conditions for ensuring frequency nadir adequacy through ex-ante dispatch instructions. A simplified dynamic model of primary frequency response was developed to formulate a constraint suitable for an optimal power flow framework. A group of authors [16], [17] studied the impact of system inertia under uncertainties associated with wind generation and unit outages. Lee and Baldick [16] modeled a two-stage stochastic frequency based ED under uncertainties of unit outages. The L-shaped method was used to solve a large stochastic program. Teng, Strbac and *et al.* [17] proposed a stochastic frequency-based UC that ensures the comprehensive frequency dynamic performance (i.e., RoCoF, frequency nadir and quasi-steady-state frequency) meets the secu-

Manuscript received September 23, 2015; revised December 16, 2015 and January 18, 2016; accepted January 24, 2016. This work was supported by the Fundamental Research Funds for the Central Universities(0903005203315). Paper no. TPWRS-01345-2015.

Y. Wen and X. Liu are with the State Key Laboratory of Power Transmission Equipment and System Security and New Technology, Chongqing University, Chongqing 400044, China (e-mail: wenyunfeng@cqu.edu.cn).

W. Li is with the State Key Laboratory of Power Transmission Equipment and System Security and New Technology, Chongqing University, Chongqing 400044, China, and also with Simon Fraser University, Vancouver, BC V5A 1S6, Canada.

G. Huang is with the College of Electrical Engineering, Zhejiang University, Hangzhou, Zhejiang 310027, China.

Color versions of one or more of the figures in this paper are available online at http://ieeexplore.ieee.org.

Digital Object Identifier 10.1109/TPWRS.2016.2521882

rity requirements. In this UC, the expected operating cost was optimized over a set of scenarios representing different realizations of wind production.

The efforts mentioned above have made significant contributions to improve the system frequency dynamics. However, the ability of a power system to maintain frequency stability still mainly relies on synchronous units with slow dynamics. If such units committed are not enough, power outputs of renewable plants must be curtailed so that more synchronous units can be run to ensure sufficient system inertia; otherwise automatic load-shedding would be triggered to restore the power equilibrium and prevent a frequency collapse [1].

The availability of emerging fast-acting energy storage technologies such as batteries and ultra-capacitors considerably increases the scope for dynamic frequency control, since these devices are able to instantly inject power to counteract system power imbalance [1], [18]. The problem of dimensioning the battery storage system to provide primary frequency reserves has been addressed in [19]. Practical projects in northern Chile [20] and some island power systems such as French Guadeloupe [21] and Spanish Cannary [22] have technically shown the feasibility of fast-response storage to improve the PFR. However, the above storage applications are based on ex post local measurement and control, they do not provide a criterion to establish frequency dynamic adequacy through ex-ante dispatch instructions. If the pre-contingency preserved energy capacity of storage units is insufficient, the scope for frequency control would be limited. Also, the single application of frequency regulation is unlikely cost effective to justify the investment of batteries.

The goal of this paper is to describe how the operation of battery energy storage for dynamic frequency support can be optimized as part of Frequency Dynamics Constrained Unit Commitment (FDUC). This problem is formulated using interval-based optimization in order to cope with the impact of uncertain wind generation on system inertia and frequency dynamics. The contributions of this paper include the following:

1) A dynamic frequency control strategy with batteries is proposed. Immediately after a generator tripping, the injections of batteries are adjusted instantly to provide a dynamic frequency support. Such actions would be able to ensure minimum system power imbalance while reducing the stress of synchronous units to provide the inertia and primary reserve.
2) Multiple applications of a battery storage are included in the proposed FDUC formulation (denoted as FDUCB) to perform energy arbitrage in the normal state, and provide dynamic frequency support following a major credible contingency. The FDUCB explicitly imposes constraints on the deliverability of system inertia and primary reserves as well as emergent fast-response storages to ensure the RoCoF adequacy and frequency nadir adequacy.
3) Application of the Reformulation-Linearization Technique (RLT) is carried out to reformulate the original nonlinear model into a Mixed-Integer Linear Programming (MILP) problem, resulting in a significant decrease in computing efforts.

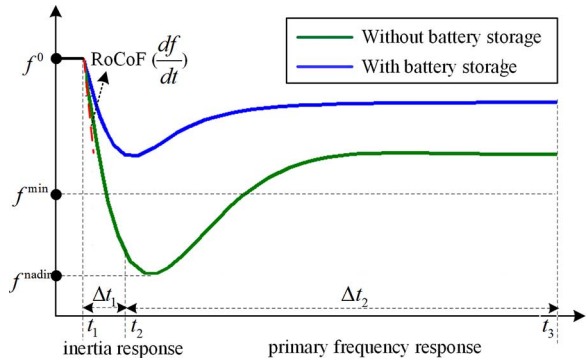

Fig. 1. Dynamic frequency response with and without battery storage.

In comparison to previous approaches, the proposed method has the following advantages:

1) It improves the system's resilience to withstand a major frequency disturbance, i.e., slowing down the RoCoF and increasing the minimum frequency without the need for wind curtailment.
2) It mitigates the inertia and PFR requirements for the synchronous units and therefore reduces the total operating cost.

The proposed technique is easily implementable in existing power systems as the batteries' post-contingency frequency-arrest actions were determined in advance.

II. Frequency Dynamics and Dynamic Frequency Control With Battery Storage

A. Frequency Dynamics

The dynamics of system frequency can be governed by the first-order swing equation [23]:

$$\frac{d\Delta f(t)}{dt} = \frac{1}{2H}(\Delta PG(t) + \Delta PS(t) - \Delta PL(t) - D \cdot \Delta f(t)) \quad (1)$$

where $\Delta f(t)$ is the frequency deviation, H [MW·s/Hz] is the system inertia after a generation loss which refers to the ability of the system to resist a frequency change following a contingency, D [1/Hz] is the load-damping rate, $\Delta PG(t)$[MW] and $\Delta PS(t)$ [MW] denotes respectively the increased power outputs from the synchronous units and battery storage units following the generation loss $\Delta PL(t)$ [MW].

A typical waveform for a post-contingency short-term frequency excursion without frequency support from battery storage is shown in Fig. 1 (green curve). During the first several seconds (Δt_1, 0–5 s), the frequency drop is only limited by the inertia response of synchronous units. After the governor dead-band, the PFR will take action deploying the primary reserve to stabilize the frequency to the quasi-steady-state setting value. The duration (Δt_2) of PFR is typically 5 to 25 s. Secondary and tertiary reserves occurring in a long-term timescale (30 s to 15 min) are beyond the scope of this paper.

During the short-term transient period, two most important metrics indicating dynamic system frequency security must be managed to prevent system collapse: 1) RoCoF [Hz/s]—the

slope of the frequency which falls immediately following a contingency; 2) Frequency nadir (f^{nadir}[Hz])—the lowest frequency reached before frequency starts to recover.

The decline of system inertia as a result of the increasing displacement of synchronous units by renewable units deteriorates the system frequency dynamics and more seriously, increases the risk of frequency collapse and blackout. Low system inertia and insufficient PFR is most likely to occur when the system is operated with low load but high wind penetration [1]. Under such scenarios, if a major unit is suddenly in outage, the RoCoF might become too high or the frequency nadir might move outside the tolerable contingency band, which would respectively trigger the RoCoF relay and Under-Frequency Load-Shedding (UFLS) relay to prevent a frequency collapse.

B. Dynamic Frequency Control With Battery Energy Storage

In the actual operation of power systems, the operator is usually obliged to maintain a sufficient amount of active power in reserve to cover the loss of the largest online generating unit [1]. Therefore, we consider this worst-case contingency for frequency dynamic analysis. The response time of battery storage is neglected because of its capability of ramping up to full output in tens to hundreds of milliseconds [18], [20], [21]. The dynamic frequency control with battery energy storage can be illustrated using Figs. 1–3:

1) Following the occurrence of the largest generation loss at time t_1, battery n immediately injects power at its full capacity $PS_n^{\text{dis,max}}$ [MW] to compensate the power imbalance. The power change ΔPS_n [MW] of a battery storage device is

$$\Delta PS_n = PS_n^{\text{dis,max}} - PS_n^{\text{dis}} + PS_n^{\text{ch}} \tag{2}$$

where PS_n^{dis} [MW] and PS_n^{ch} [MW] are respectively the base case discharge and charge power of battery n. The original power imbalance $\Delta PL^{\max}$ of the system is instantly reduced to:

$$\Delta PL' = \Delta PL^{\max} - \sum_n \Delta PS_n \tag{3}$$

2) The power injection from the batteries remains constant during the short-term transient period until the required PFR of synchronous units have been fully activated.
3) During the inertia response timeframe Δt_1, the power imbalance keeps constant at $\Delta PL'$. After the governor deadband, synchronous units start deploying PFR with a constant rate and the power imbalance during the PFR timeframe Δt_2 decreases linearly until it reaches zero in the quasi-steady-state.

According to (2), the maximum possible power change of a battery storage device following a credible contingency is $PS_n^{\text{dis,max}} + PS_n^{\text{ch,max}}$, which occurs when the battery is charged at the maximum limit ($PS_n^{\text{ch,max}}$ [MW]) in the normal operation. The corrective actions from batteries could thus back-up a considerable amount of power imbalance, and consequently reduce the requirements of inertia and primary

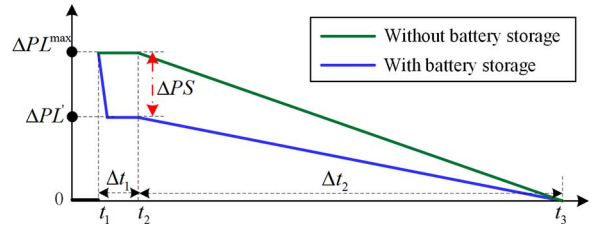

Fig. 2. System power imbalance as a function of time.

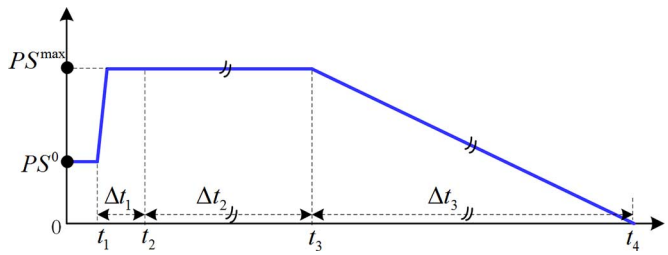

Fig. 3. Power injection of the battery storage as a function of time.

reserve from conventional synchronous units. In comparison with the frequency excursion curve without battery storage, the dynamic frequency support from batteries (Fig. 1, blue curve) guarantees the frequency stability, i.e., slowing down the RoCoF and ensuring the frequency nadir within the tolerable contingency band.

Although we do not consider the generators' Secondary Frequency Response (SFR), it is necessary to avoid the batteries causing a sudden power imbalance during the SFR timeframe (Δt_3, typically 5 min). After the system has recovered from a previous disturbance via inertia response and PFR, the batteries are required to continuously reduce their injections to zero until the AGC actions have been fully deployed (as shown in Fig. 3). Therefore, the amount of energy ΔE_n [MWh] that a battery storage device must be able to discharge to help deal with the post-contingency frequency deviation is:

$$\begin{aligned}\Delta E_n &= PS_n^{\text{dis,max}}(\Delta t_1 + \Delta t_2) + 0.5 PS_n^{\text{dis,max}} \Delta t_3 \\ &= PS_n^{\text{dis,max}}(\Delta t_1 + \Delta t_2 + 0.5\Delta t_3)\end{aligned} \tag{4}$$

Note that if the penetration level of the installed batteries is sufficiently high, i.e., the total power capacity of the storages is greater than or equals to the largest generation loss $\Delta PL^{\max}$, the immediate power imbalance $\Delta PL^{\max}$ can be fully compensated by the batteries' injections:

$$\Delta PL^{\max} = \sum_n \Delta PS_n = \sum_n (PS_n^{\text{dis}'} - PS_n^{\text{dis}} + PS_n^{\text{ch}}) \tag{5}$$

where $PS_n^{\text{dis}'}$ [MW] is the post-contingency discharging power of battery n. In this case, the pre-contingency frequency is almost maintained since the actual power imbalance can be reduced to zero ($\Delta PL' = 0$). The amount of energy ΔE_n that battery n must deliver to deal with the contingency is:

$$\Delta E_n = PS_n^{\text{dis}'}(\Delta t_1 + \Delta t_2 + 0.5\Delta t_3) \tag{6}$$

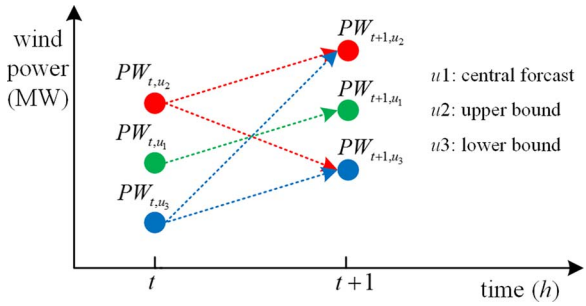

Fig. 4. Scenarios with inter-hour transition constraints.

III. Problem Formulation

In order to guarantee the dynamic frequency security following a credible contingency, the FDUCB formulation enforces not only the operating limits in the nominal state, but also the synchronous units' primary reserve requirements as well as the storage units' corrective actions for post-contingency inertia response and primary frequency control. In addition, the battery storage's ability to provide a dynamic frequency control is interacted economically with the energy arbitrage benefits it can provide. The multiple applications of battery storage can reduce the operating cost and help justify the investment of this new technology.

A. Wind Uncertainty Modelling

The interval optimization [24] is used to deal with the impacts of wind uncertainty on unit scheduling and frequency dynamics. Unlike the scenario-based optimization [17], the interval optimization does not require sampling scenarios from a presumed probability distribution for wind uncertainties. Instead, the generation uncertainty of each wind farm is represented by three non-probabilistic scenarios as depicted in Fig. 4: the central forecast u_1 (green circles), the upper bound u_2 (red circles) and the lower bound u_3 (blue circles). The FDUCB must ensure the feasibility of transitions from the lower to upper bound, and vice versa, between any two consecutive time periods. Such inter-hour transitions include not only the up/down ramping of generators but also the variation in State-of-Charge (SoC) of batteries.

B. FDUCB Model

In the following equations, the indices i, m, n, b, u and t refer to the sets of synchronous units, wind farms, battery storage units, load buses, scenarios and time intervals, respectively.

The objective function of the FDUCB aims to minimize the overall operating cost of the central forecast scenario (u_1) over the scheduling horizon with a 1-hour time resolution:

$$\text{Min} \sum_t \sum_i \left(SU_{t,i} + F_i x_{t,i} + \sum_j c^{\text{G}}_{i,j} p_{t,i,j,u_1} + c^{\text{R}}_i R_{t,i,u_1} \right) + \sum_t \sum_n c^{\text{B}}_n \left(PS^{\text{dis}}_{t,n,u_1} + PS^{\text{ch}}_{t,n,u_1} \right) \quad (7)$$

The first four items in (7) represent the operating cost of the generators, which consists of the startup cost $SU_{t,i}$ [\$], the no-load cost $F_i x_{t,i}$, the running cost (represented by a three-segment piecewise linear approximation of the convex cost curve), and the cost for providing primary reserve. $x_{t,i}$ denotes the on/off status of generator i at hour t, p_{t,i,j,u_1} [MW] is the power produced by generator i on segment j of its cost curve at hour t, R_{t,i,u_1} [MW] is the primary reserve of generator i at hour t, $c^{\text{G}}_{i,j}$ is the marginal cost of generator i on segment j, c^{R}_i is the cost offer of the primary reserve provided by generator i. The last item in (7) represents the batteries' operating cost. $PS^{\text{dis}}_{t,n,u_1}$ [MW] and PS^{ch}_{t,n,u_1} [MW] respectively represent the discharging and charging power of battery n at hour t. The battery operating cost model proposed in [25] is adopted, in which the MWh price c^{B}_n accounts for battery degradation due to charging/discharging cycles. See the Appendix Section for detailed explanation.

This optimization is subject to the constraints given in Sections III-B1 and III-B2 below. The constraints given in Section III-B1 pertain to the base case optimization of the schedule of the generators and storage units. The constraints given in Section III-B2 pertain to the post-contingency frequency dynamics management when the power capacity of the installed batteries is relatively small in comparison with the largest generation loss. The related constraints for the FDUCB with high penetration of battery storages $(\Delta PL^{\max} - \sum_n \Delta PS_n = 0)$ is described in Section III-C.

1) Constraints for the Nominal Operation: In the nominal state, the FDUCB determines a set of unit on/off status variables which are feasible for all possible scenarios. For each scenario, there is a set of generators' power outputs and a set of batteries' charging/discharging powers.

• *Operation Constraints of the Generators:*

$$\forall t, \forall i, \forall u: \quad PG_{t,i,u} = \sum_j p_{t,i,j,u}, 0 \le p_{t,i,j,u} \le p^{\max}_{i,j} \cdot x_{t,i} \quad (8)$$

$$\forall t, \forall i, \forall u: \quad PG_{t,i,u} \ge PG^{\min}_i \cdot x_{t,i} \quad (9)$$

$$\forall t, \forall i: \quad -RD_i \le PG_{t,i,u} - PG_{t-1,i,u} \le RU_i \quad (10)$$

$$\forall t, \forall i: \quad PG_{t-1,i,u_2} - PG_{t,i,u_3} \le RD_i \quad (11)$$

$$\forall t, \forall i: \quad -PG_{t-1,i,u_3} + PG_{t,i,u_2} \le RU_i \quad (12)$$

Constraints (8) and (9) enforce the operating limits of generators. $PG_{t,i,u}$ [MW] represents the power output of the i-th generator following scenario u at hour t, $p^{\max}_{i,j}$ [MW] is the length of segment j of the output curve of generator i, $PG^{\min}_i$ [MW] is the minimum output limit of generator i. Constraints (10)–(12) enforce the feasibility of inter-hour ramping transitions in a given uncertainty range, as illustrated in Fig. 4. Constraint (10) enforces both the up (RU_i [MW]) and down (RD_i [MW]) ramp limits on the scenarios. Constraint (11) enforces the ramping transition requirement from the upper bound (at hour $t-1$) to the lower bound (at hour t), while constraint (12) enforces the ramping transition requirement from the lower bound (at hour $t-1$) to the upper bound (at hour t). Ramping constraints from the central forecast to the lower and upper bound scenarios are excluded since they hold automatically because of constraints (11) and (12) [24].

The minimum up/down time and stair-startup cost limits of the generating units are also included. The detailed formulation can be found in the authors' previous work [26].

• *Operation Constraints of the Batteries:* See (13)–(19) at the bottom of the page. Constraints (13) and (14) denote the minimum and maximum limits on the charging and discharging powers. Binary variable $Q^{\text{ch}}_{t,n,u}$ is equal to 1 when battery n is being charged, and 0 otherwise. Constraint (15) calculates the energy $E_{t,n,u}$ [MWh] stored in each storage unit at hour t. α is the energy dissipation rate, η^{ch}_n and η^{dis}_n are respectively the charging and discharging efficiencies of battery storage n. To preserve the lifetime of battery storage facilities, the stored energy can be kept above a particular percentage of the capacity [27], which can be expressed as the maximum Depth of Discharge ($DoD^{\max}$). Constraint (16) enforces that the State of Charge (SoC) of each battery storage device exists between the minimum allowed level and its rated capacity $E^{\max}_n$ [MWh]. Constraints (17) and (18) enforce the feasibility of inter-hour SoC transitions between the upper and lower bounds. Constraint (19) sets the final SoC scenarios of each battery storage device to be a pre-specified value, which is commonly chosen to be equal to the initial value.

• *Transmission Constraints:* See (20) and (21) at the bottom of the page. Constraint (20) imposes the total power injection from the generators, wind plants and batteries to meet the total load demand. $PW_{t,m,u}$ [MW] denotes the power output of the m-th wind farm following scenario u at hour t. $PD_{t,b}$ [MW] denotes the hourly load demand at bus b. Constraint (21) enforces the branch flows of transmission lines within their maximum limits $\mathrm{F}^{\max}$ [MW] via a linear dc power flow model. SF is the shift factor matrix. K^{G}, K^{W}, K^{S} and K^{D} are respectively the bus-generator, bus-wind, bus-storage, and bus-load incidence matrices.

If no battery is considered in the FDUC formulation, wind curtailments would be enforced in the normal operation so as to: i) avoid infeasibility of the transmission constraints (20)–(21); ii) and allow more synchronous units to be committed to ensure post-contingency frequency stability.

2) Constraints for the Post-Contingency Frequency Dynamics Management: The generators' on/off status and primary reserve, along with the batteries' instant corrective actions must be co-optimized to manage the post-contingency RoCoF and frequency nadir metrics under all scenarios.

• *System Power Imbalance:* Immediately after the contingency, the batteries will release additional power to reduce the generation loss. The remaining power imbalance $\Delta PL^{'}_{t,u}$ [MW] is determined by the (22) at the bottom of the page.

$$\forall t,\forall n,\forall u: \quad 0 \le PS^{\text{ch}}_{t,n,u} \le PS^{\text{ch,max}}_{n} Q^{\text{ch}}_{t,n,u} \tag{13}$$

$$\forall t,\forall n,\forall u: \quad 0 \le PS^{\text{dis}}_{t,n,u} \le PS^{\text{dis,max}}_{n} (1 - Q^{\text{ch}}_{t,n,u}) \tag{14}$$

$$\forall t,\forall n,\forall u: \quad E_{t,n,u} = (1-\alpha)E_{t-1,n,u} + \eta^{\text{ch}}_n PS^{\text{ch}}_{t,n,u} - \frac{1}{\eta^{\text{dis}}_n} PS^{\text{dis}}_{t,n,u} \tag{15}$$

$$\forall t,\forall n,\forall u: \quad (1-DoD^{\max})E^{\max}_n \le E_{t,n,u} \le E^{\max}_n \tag{16}$$

$$\forall t,\forall n: \quad (1-DoD^{\max})E^{\max}_n \le (1-\alpha)E_{t-1,n,u_2} + \eta^{\text{ch}}_n PS^{\text{ch}}_{t,n,u_3} - \frac{1}{\eta^{\text{dis}}_n} PS^{\text{dis}}_{t,n,u_3} \le E^{\max}_n \tag{17}$$

$$\forall t,\forall n: \quad (1-DoD^{\max})E^{\max}_n \le (1-\alpha)E_{t-1,n,u_3} + \eta^{\text{ch}}_n PS^{\text{ch}}_{t,n,u_2} - \frac{1}{\eta^{\text{dis}}_n} PS^{\text{dis}}_{t,n,u_2} \le E^{\max}_n \tag{18}$$

$$\forall n,\forall u: \quad E_{t_T,n,u} = E_{t_0,n} \tag{19}$$

$$\forall t,\forall u: \sum_i PG_{t,i,u} + \sum_m PW_{t,m,u} + \sum_n PS^{\text{dis}}_{t,n,u} - \sum_n PS^{\text{ch}}_{t,n,u} = \sum_b PD_{t,b} \tag{20}$$

$$\forall t,\forall u: -\mathrm{F}^{\max} \le \mathrm{SF}\left[\mathrm{K}^{\mathrm{G}}\mathrm{PG}_{t,u} + \mathrm{K}^{\mathrm{W}}\mathrm{PW}_{t,u} + \mathrm{K}^{\mathrm{S}}\left(\mathrm{PS}^{\text{dis}}_{t,u} - \mathrm{PS}^{\text{ch}}_{t,u}\right) - \mathrm{K}^{\mathrm{D}}\mathrm{PD}_t\right] \le \mathrm{F}^{\max} \tag{21}$$

$$\forall t,\forall u: \quad \Delta PL^{'}_{t,u} = \Delta PL^{\max} - \sum_n \left(PS^{\text{dis,max}}_{n} - PS^{\text{dis}}_{t,n,u} + PS^{\text{ch}}_{t,n,u}\right) \tag{22}$$

• *RoCoF Limit:* The post-contingency initial RoCoF is proportional to the size of the actual power imbalance and inversely proportional to the quantity of system inertia [1], [13], [17]:

$$\forall t, \forall u: \quad RoCoF = \frac{d\Delta f(t)}{dt} = \frac{\Delta PL'_{t,u}}{2H_{t,u}} \leq RoCoF^{\max} \tag{23}$$

Inertia response of the synchronous units and corrective actions from the batteries' must be operationally managed to ensure that the initial RoCoF does not exceed a limit ($RoCoF^{\max}$ [Hz/s]) that can trigger a RoCoF relay. Since the post-contingency system inertia level $H_{t,u}$ is a function of the remaining online generating units, the unit status should be optimized to ensure that sufficient generating units are online to provide an inertia response. Based on this point, the constraint (23) can be rewritten as [17]:

$$\forall t, \forall u: H_{t,u} = \frac{\sum\limits_{i, i \neq L} H_i \cdot PG_i^{\max} \cdot x_{t,i}}{f^0} \geq \frac{\Delta PL'_{t,u}}{2RoCoF^{\max}} \tag{24}$$

where H_i [s] denotes the inertia constant of generator i, f^0 [Hz] is the base case frequency.

• *Frequency Nadir Limit:* The frequency nadir depends on system inertia, governor's response and batteries' fast corrective actions. The sufficient conditions for ensuring the primary response adequacy proposed in [15] are used to ensure that the frequency nadir will not drop below a pre-specified limit $f^{\min}$ that can trigger a UFLS relay:

$$\forall t, \forall i, \forall u: \quad R_{t,i,u} \leq 2v_i \frac{H_{t,u}\left(f^0 - f^{\min} - f^{\mathrm{db}}\right)}{\Delta PL'_{t,u}} \tag{25}$$

$$\forall t, \forall u: \quad \sum_i R_{t,i,u} \geq \Delta PL'_{t,u} \tag{26}$$

where f^{db} [Hz] is the governors' dead band, v_i [MW/s] is the maximum governor ramp rate of generator i. Constraint (25) ensures that the primary reserve of each generator can be delivered at or before the time when the frequency nadir occurs. Constraint (26) ensures that the amount of primary reserve provided by the remaining online synchronous units is enough to cover a contingency of size $\Delta PL'_{t,u}$.

• *Contingency SoC Limits of the Batteries:*

$$\forall t, \forall n, \forall u: \ 0 \leq E'_{t,n,u} = (1-\alpha)E_{t,n,u} - \Delta E_{t,n,u} \leq E_n^{\max} \tag{27}$$

This constraint accounts for the post-contingency storage dynamics and ensures that the SoC of each storage unit in the normal state is sufficient to deal with the frequency disturbance. Since the loss of the largest generating unit is a rare event, the minimum limit of the post-contingency SoC ($E'_{t,n,u}$) can be relaxed to be zero.

• *Primary Reserve Limits of the Synchronous Units:*

$$\forall t, \forall i, \forall u: \quad 0 \leq R_{t,i,u} \leq R_i^{\max} \tag{28}$$

$$\forall t, \forall i, \forall u: \quad PG_{t,i,u} + R_{t,i,u} \leq PG_i^{\max} \cdot x_{t,i} \tag{29}$$

Constraint (28) imposes the lower and upper limits on the primary reserve provided by each generator. Constraint (29) ensures the primary reserve amount of each generator not to exceed the allowed spinning headroom that can contribute to primary frequency response provision.

C. Remarks on the FDUCB

The proposed dynamic frequency control strategy is able to correct the credible contingency without causing frequency excursion when the penetration level of storages is sufficiently high ($\Delta PL^{\max} - \sum\limits_n \Delta PS_n = 0$). In this case, the operation constraints for the post-contingency frequency dynamic control should be reduced so that the FDUCB model only has to enforce the constraints (5), (6) and (27), along with the base case constraints (8)–(21) as well as the minimum up/down time and stair-startup cost limits of the units.

The load-damping effect is usually ignored by other researchers when performing frequency dynamic analysis [1], [3], [4], [13], [15] since the post-contingency frequency deviation caused by the load-damping during the short-term transient period is relatively small and bounded. Neglecting this effect is generally an acceptable assumption.

The post-contingency transmission constraints are not incorporated in the model as the transmission lines can be overloaded for a short period of time after a contingency due to their emergency ratings [18], [28], whose timeframe is usually longer than the frequency dynamic period.

IV. Solution Technique

The FDUCB model described in Part C of Section III is an MILP and can be solved easily with help of a commercial solver, such as CPLEX.

However, the FDUCB model described in Part B of Section III (the total power capacity of the installed batteries is relatively small) cannot be solved directly using MILP because of the only nonlinear constraint (25). This section explains how the nonlinear terms in this constraint can be avoided using the Reformulation-Linearization Technique (RLT). The RLT is a unifying approach for solving wide classes of discrete and continuous factorable nonconvex optimization problems through the generation of tight effective relaxations in a higher dimensional space [29]. The RLT can be applied to remove the nonlinear terms in constraint (25) because 1) the nonlinear terms ($R_{t,i,u}PS^{\mathrm{dis}}_{t,n,u}$ and $R_{t,i,u}PS^{\mathrm{ch}}_{t,n,u}$) are in the form of bilinear products; 2) all the variables ($PS^{\mathrm{dis}}_{t,n,u}$, $PS^{\mathrm{ch}}_{t,n,u}$ and $R_{t,i,u}$) are bounded. The reformulation procedure is described as following:

Step 1) Transform constraint (25) as shown in (30) at the bottom of the next page.

Step 2) Reformulate the bilinear products via substituting $R_{t,i,u}PS^{\mathrm{ch}}_{t,n,u}$ and $R_{t,i,u}PS^{\mathrm{dis}}_{t,n,u}$ by using the auxiliary, nonnegative and continuous variables $A^{\mathrm{ch}}_{t,i,n,u}$ and $A^{\mathrm{dis}}_{t,i,n,u}$.

Step 3) Finally, the McCormick's envelope [29] is used to bound $A^{\mathrm{ch}}_{t,i,n,u}$ and $A^{\mathrm{dis}}_{t,i,n,u}$. See (31)–(36) at the bottom of the page.

After employing the above linearization technique, the original nonlinear FDUCB is reformulated as an MILP problem and can be solved using CPLEX. See the Appendix Section for the mathematical explanation of the RLT.

V. Case Study

A six-bus system and the modified IEEE RTS-79 system are applied to illustrate the performance of the proposed FDUCB. The following same parameters are assumed for the two systems: i) the wind power uncertainty is assumed to be 20% of its central forecast (u_1), i.e., the upper bound (u_2) and lower bound (u_3) of wind power are respectively 120% and 80% of its central forecast; ii) The maximum depth of discharge is set at 90% and the energy dissipation rate is 0; iii) the system base case frequency f^0 is 50 Hz, and the governors' dead-band is 20 mHz; iv) the time length of inertia response, PFR and SFR are respectively 5 s, 25 s and 5 min. The performance of the FDUCB described by (7)–(29) is compared with the following three UC schemes that do not include any battery storage:

1) CUC: UC with simple capacity-based PFR constraints, which are described by (8)–(12), (20)–(22), (26), (28), (29) and the minimum up/down time and stair-startup cost limits of the generating units.
2) FDUC-I: CUC with frequency dynamic constraints (24) and (25) but without wind curtailment actions.
3) FDUC-II: FDUC-I with wind curtailments in the normal state.

All the four UC formulations use interval numbers to model wind power uncertainty. The numerical tests were performed on GAMS 24.1 platform using the CPLEX12.1 MILP solver. The MATLAB/SIMULINK model was built up to simulate the frequency dynamic performance of the four models. All the data used for the optimization and the frequency domain models in the simulations are available at [30].

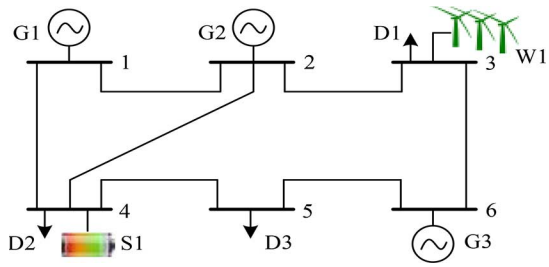

Fig. 5. Six-bus system.

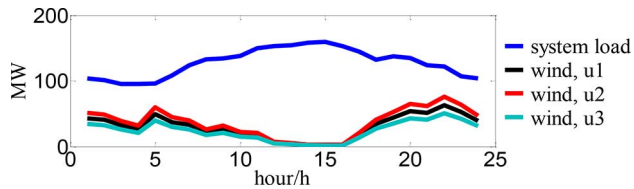

Fig. 6. Aggregated load profile and wind scenarios.

A. Six-Bus System

The system diagram is depicted in Fig. 5, a wind farm is located at bus 3 and a 2 MW/2 MWh battery storage device is installed at bus 4. The aggregated load profile and wind power scenarios with a 24-h horizon are shown in Fig. 6. The minimum allowed frequency is set at 49.5 Hz and the maximum RoCoF is set at 0.5 Hz/s. The inertia constants of generators G1, G2 and G3 are 5 s, 3 s and 4 s, respectively. For clarity, the contingency event of this small system is assumed to be a sudden increase of 10% of the total load. The MIP gap is set at 0.1%.

Table I compares the solutions obtained in the four cases. *TC* is the total operating cost, *CG* and *CR* are respectively the synchronous units' generation cost and primary reserve cost, *CB* is the battery storage unit operation cost, and *TW* is the total curtailed wind power. CUC is the cheapest scheme but would result in a potential frequency collapse following a contingency because it does not enforce the frequency dynamic security constraints. The FDUC-I failed to find any feasible solution because

$$\begin{aligned}&\forall t,\forall i,\forall u: \quad R_{t,i,u}\Delta PL'_{t,u}\\&= R_{t,i,u}\Delta PL^{\max}-\sum_n R_{t,i,u}PS_n^{\mathrm{dis,max}}+\sum_n R_{t,i,u}PS^{\mathrm{dis}}_{t,n,u}-\sum_n R_{t,i,u}PS^{\mathrm{ch}}_{t,n,u}\\&\le 2v_iH_{t,u}\left(f^0-f^{\min}-f^{\mathrm{db}}\right)\end{aligned}\tag{30}$$

$$\begin{aligned}&\forall t,\forall i,\forall n,\forall u:\\&A^{\mathrm{ch}}_{t,i,n,u}-R^{\max}_{t,i,u}PS^{\mathrm{ch}}_{t,n,u}-PS^{\mathrm{ch,max}}_{t,n,u}R_{t,i,u}+R^{\max}_{t,i,u}PS^{\mathrm{ch,max}}_{t,n,u}\ge 0 &(31)\\&-A^{\mathrm{ch}}_{t,i,n,u}+PS^{\mathrm{ch,max}}_{t,n,u}R_{t,i,u}\ge 0 &(32)\\&-A^{\mathrm{ch}}_{t,i,n,u}+R^{\max}_{t,i,u}PS^{\mathrm{ch}}_{t,n,u}\ge 0 &(33)\\&A^{\mathrm{dis}}_{t,i,n,u}-R^{\max}_{t,i,u}PS^{\mathrm{dis}}_{t,n,u}-PS^{\mathrm{dis,max}}_{t,n,u}R_{t,i,u}+R^{\max}_{t,i,u}PS^{\mathrm{dis,max}}_{t,n,u}\ge 0 &(34)\\&-A^{\mathrm{dis}}_{t,i,n,u}+PS^{\mathrm{dis,max}}_{t,n,u}R_{t,i,u}\ge 0 &(35)\\&-A^{\mathrm{dis}}_{t,i,n,u}+R^{\max}_{t,i,u}PS^{\mathrm{dis}}_{t,n,u}\ge 0 &(36)\end{aligned}$$

TABLE I
SOLUTIONS PRODUCED BY THE FOUR VARIANTS OF UC WITH 0.1% MIP GAP

Model	*TC* $	*CG* $	*CR* $	*CB* $	*TW* MW	Time s
CUC	57,156	55,930	1,226	---	---	5
FDUC-I	Failed to produce feasible solutions.					
FDUC-II	66,801	65,575	1,226	---	65.78	19
FDUCB	59,315	58,227	1,031	57	---	10

TABLE II
HOURLY COMMITTED GENERATING UNITS PRODUCED BY CUC

G	1	2	3	4	5	6	7	8	9	10	11	12	13	14	15	16	17	18	19	20	21	22	23	24
1	1	1	1	1	1	1	1	1	1	1	1	1	1	1	1	1	1	1	1	1	1	1	1	1
2	0	0	0	0	0	0	1	1	1	1	1	1	1	1	1	1	1	1	1	1	1	0	0	0
3	0	0	0	0	0	0	0	0	0	0	0	0	0	0	0	0	0	0	0	0	0	0	0	0

TABLE III
HOURLY COMMITTED GENERATING UNITS PRODUCED BY FDUC-II

G	1	2	3	4	5	6	7	8	9	10	11	12	13	14	15	16	17	18	19	20	21	22	23	24
1	1	1	1	1	1	1	1	1	1	1	1	1	1	1	1	1	1	1	1	1	1	1	1	1
2	1	1	1	1	1	1	1	1	1	1	1	1	1	1	1	1	1	1	1	1	1	1	1	1
3	0	0	0	0	0	0	1	1	1	1	1	1	1	1	1	1	1	1	1	1	1	1	0	0

wind curtailments are not enforced in the base case and as a result, the committed units cannot provide sufficient inertia and PFR to meet the frequency security constraints (24) and (25). The FDUC-II ensures the frequency security at the expense of curtailing 65.78 MW wind generation during low-demand periods with high wind generation, i.e., 3.58 MW wind generation is curtailed at hour 5 and 62.2 MW at hour 22. Moreover, inclusion of the frequency dynamic security constraints (both RoCoF and frequency nadir) in the UC formulation remarkably increases the cost of dispatching the system for the day: a 16.87% increase in the total cost can be seen compared with the CUC. The FDUCB obtains a solution that is more expensive than the CUC but much cheaper than the FDUC-II. Compared with the FDUC-II, the proposed FDUCB requires a smaller amount of primary reserve and no wind generation curtailment to meet the frequency dynamic security.

The resulting schedules of synchronous units produced by the CUC, FDUC-II and FDUCB are summarized in Tables II to IV. Table II indicates that the CUC performs the most economic scheduling via turning off the expensive generator G3 throughout the day. The results of Table III show that inclusion of frequency dynamic constraints in the UC formulation calls for more synchronous units being turned on to provide sufficient inertia and primary reserve. In comparison with the CUC, in FDUC-II, generator G2 is committed every hour and generator G3 must be turned on during hour 7 to 22. This is the reason why FDUC-II has a very expensive operating cost. Table IV shows that the FDUCB significantly mitigates the inertia and PFR requirements for the synchronous units as a result of the dynamic frequency support provided by the 2 MW/2 MWh battery storage. Minimum synchronous units are needed to commit in almost the whole day except for peak load hours 13 to 15.

Figs. 7 and 8 show the hourly post-contingency frequency dynamic metrics (*RoCoF* and f^{nadir}) calculated using the so-

TABLE IV
HOURLY COMMITTED GENERATING UNITS PRODUCED BY FDUCB

G	1	2	3	4	5	6	7	8	9	10	11	12	13	14	15	16	17	18	19	20	21	22	23	24
1	1	1	1	1	1	1	1	1	1	1	1	1	1	1	1	1	1	1	1	1	1	1	1	1
2	0	0	0	0	0	0	1	1	1	1	1	1	1	1	1	1	1	1	1	1	1	1	0	0
3	0	0	0	0	0	0	0	0	0	0	0	0	1	1	1	0	0	0	0	0	0	0	0	0

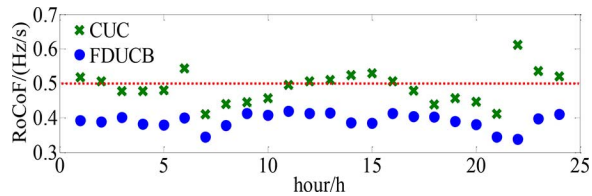

Fig. 7. Initial RoCoF following the contingency at each hour produced by the CUC and FDUCB.

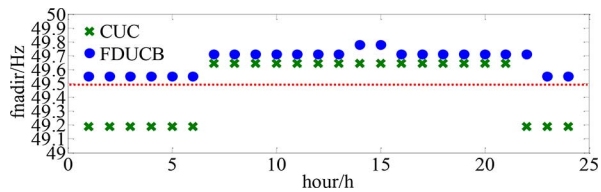

Fig. 8. Frequency nadir following the contingency at each hour produced by the CUC and FDUCB.

lutions produced by the CUC and FDUCB. The conventional capacity-based method (CUC) doesn't satisfy the RoCoF and frequency nadir limits in most overnight hours with high wind and low load as it only relies on generator G1 to provide inertia in these hours. On one hand, the post-contingency RoCoF for CUC would exceed the maximum limit ($RoCoF^{\max} = 0.5$ Hz/s) in high wind hours 1, 2, 6, 22-24 and peak load hours 12-16. The maximum post-contingency RoCoF violation (0.61) occurs in hour 22 when the wind penetration is extremely high (around 50%) but the load is relatively low. On the other hand, the post-contingency frequency nadir for CUC would go beyond the minimum allowed frequency ($f^{\min} = 49.5$ Hz) in overnight hours 1-6 and 22-24. Leveraging corrective actions from the battery storage, FDUCB is resilient to frequency disturbances occurring in any hours of the day. As seen from Figs. 7 and 8, the post-contingency RoCoF and frequency nadir produced by the FDUCB both meet the tolerable limits well in all the hours.

Fig. 9 compares the frequency dynamics produced by the CUC and FDUCB within 30 s after a 10% load increase at hour 22. For CUC, the frequency drops sharply immediately following the contingency and declines by almost 0.8 Hz at the nadir. Such a dramatic violation of the frequency dynamic limit would trigger the RoCoF/UFLS relays and result in load shedding. By contrast, the FDUCB effectively protects the frequency dynamics; the initial RoCoF is mitigated and the frequency nadir is raised up to 49.71 Hz. This improvement of frequency dynamics is obtained by the post-contingency instant back-up power from the battery storage unit.

B. RTS-79 System

The proposed FDUCB was also tested on the modified RTS-79 system. The maximum wind penetration is assumed to

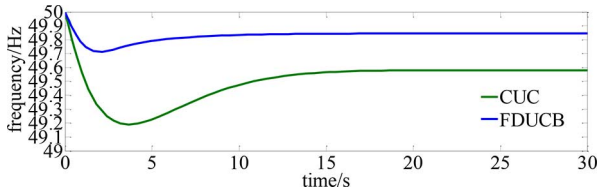

Fig. 9. Post-contingency frequency excursion curves at hour 22 produced by the CUC and FDUCB.

TABLE V
SOLUTIONS PRODUCED BY THE THREE VARIANTS OF UC WITH 0.5% MIP GAP

Model	*TC* $	*CG* $	*CR* $	*CB* $	*TW* MW	Time s
CUC	994,252	955,852	38,400	---	---	29
FDUC-II	1,167,144	1,128,744	38,400	---	716	40
FDUCB	1,068,680	1,033,855	33,545	1,280	---	120

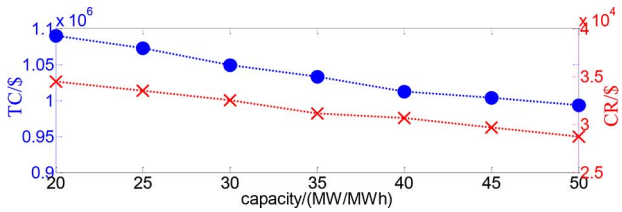

Fig. 10. Total operating cost and primary reserve cost achieved by the FDUCB as a function of battery capacity.

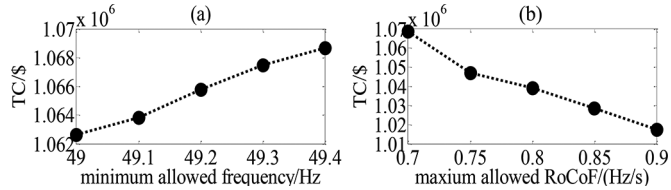

Fig. 11. (a) Total operating cost achieved by the FDUCB as a function of the minimum allowed frequency. (b) Total operating cost achieved by the FDUCB as a function of the maximum allowed RoCoF.

TABLE VI
FREQUENCY DYNAMIC METRICS ACHIEVED BY THE FDUCB FOR DIFFERENT VALUES OF THE MINIMUM ALLOWED FREQUENCY ($RoCoF^{\max} = 0.7$ HZ/S)

Metrics	fmin1= 49.4Hz	fmin2= 49.3Hz	fmin3= 49.2Hz	fmin4= 49.1Hz	fmin5= 49Hz
RoCoF	0.67	0.7	0.69	0.7	0.7
fnadir	49.6	49.59	49.58	49.56	49.55

TABLE VII
FREQUENCY DYNAMIC METRICS ACHIEVED BY THE FDUCB FOR DIFFERENT VALUES OF THE MAXIMUM ALLOWED ROCOF ($f^{\min} = 49.4$ HZ)

Metrics	rocof1= 0.7Hz/s	rocof2= 0.75Hz/s	rocof3= 0.8Hz/s	rocof4= 0.85Hz/s	rocof5= 0.9Hz/s
RoCoF	0.67	0.73	0.75	0.80	0.81
fnadir	49.63	49.62	49.62	49.61	49.6

be 20% of the peak load. Two 25 MW/25 MWh battery storage devices are installed at bus 13 and 14, respectively. The two largest nuclear units are assumed to serve the base load and the trip of one unit is considered. The minimum allowed frequency is set at 49.4 Hz and the maximum RoCoF is set at 0.7 Hz/s.

Table V compares the results obtained with the three variants of UC when the MIP gap was set at 0.5%. Both FDUC-II and FDUCB could ensure the frequency dynamics. However, the FDUC-II needs a higher operating cost and has to curtail 716 MW wind generation. FDUCB has enough storage resources to guarantee the frequency security while still preserving the economy: it achieves a cost that is slightly higher but very close to that required by the CUC. The saving from improving the scheduling cost can represent an economic incentive to use battery storage units. The last column in Table V shows that including the frequency dynamic requirements and the storage units in the optimization increases the computing time.

The value of the FDUCB depends on the power and energy capacity of battery storage units. Fig. 10 shows how the total operating cost and primary reserve cost vary as the capacity of each installed battery is increased from 20 MW/20 MWh to 50 MW/50 MWh. As the storage capacity increases, both the total operating cost and primary reserve cost are reduced. Note that the operating cost could be significantly reduced if the system has a high penetration of storages. For example, when the capacity of each battery storage is 200 MW/100 MWh, the generation loss can be fully compensated by the back-up power support from these storages, and the total operating cost is reduced to 929,873 $.

The minimum frequency limit and especially the RoCoF limit affect the total operating cost. As shown in Fig. 11, the operating cost is decreased if these frequency dynamic limits are relaxed, i.e., the setting value of the minimum frequency is decreased and the RoCoF setting value is increased. Note that there are arguments on relaxing the setting values of the existing RoCoF and minimum frequency limits for protection relays in a system with high penetration of wind generation. A careful selection of the setting levels to balance operating costs and frequency stability is essential.

Post-contingency frequency dynamic metrics following the worst scenario at hour 5, which are achieved by the FDUCB for different values of $f^{\min}$ and $RoCoF^{\max}$, are shown in Tables VI and VII. It can be seen that a smaller frequency nadir is obtained as the minimum allowed frequency is relaxed (when $RoCoF^{\max}$ is fixed at 0.7 Hz), whereas on the other hand, a larger initial RoCoF and smaller frequency nadir are obtained as the maximum allowed RoCoF is relaxed (when $f^{\min}$ is fixed at 49.4 Hz).

VI. CONCLUSION

A novel frequency dynamic constrained unit commitment (FDUCB) including corrective actions of battery storage devices for dynamic frequency support is proposed in this paper. An interval-based optimization method is used to cope with the impacts of wind uncertainty on unit scheduling and system frequency dynamics. The nonlinearity in the proposed model is handled using a reformulation-linearization technique. Case studies demonstrate that the provision of dynamic frequency control from storage units reduces the system operating cost, avoids wind curtailments and guarantees frequency security.

The proposed technique is also applicable to the sudden disconnection of large loads. In order to address the over-frequency

$$E_n^{\mathrm{tc}} = E_n^{\max} DOD^{\max} \left[LF_n^{\max} - \frac{0.2}{LF_n^{\max}} (1 + 2 + \cdots + LF_n^{\max}) \right] = E_n^{\max} DOD^{\max} (0.9 LF_n^{\max} - 0.1) \quad \text{(A3)}$$

$$(x_i - x_i^{\min})(y_j - y_j^{\min}) \geq 0 \Rightarrow A_{ij} - y_j^{\min} x_i - x_i^{\min} y_j + x_i^{\min} y_j^{\min} \geq 0$$
$$(x_i - x_i^{\min})(y_j^{\max} - y_j) \geq 0 \Rightarrow -A_{ij} + y_j^{\max} x_i - x_i^{\min} y_j^{\max} + x_i^{\min} y_j \geq 0$$
$$(x_i^{\max} - x_i)(y_j - y_j^{\min}) \geq 0 \Rightarrow -A_{ij} + x_i^{\max} y_j - x_i^{\max} y_j^{\min} + y_j^{\min} x_i \geq 0$$
$$(x_i^{\max} - x_i)(y_j^{\max} - y_j) \geq 0 \Rightarrow A_{ij} + x_i^{\max} y_j^{\max} - x_i^{\max} y_j - y_j^{\max} x_i \geq 0 \quad \text{(A4)-(A7)}$$

dynamic issues, the batteries must be charged to absorb the excessive generation until the contingency reserves become fully effective. More discussions on this topic may be considered in the future work.

APPENDIX

A. Battery Operating Cost Model

The equations representing the battery operating cost model in [25] are as follows:

$$C_n^{\mathrm{B}} = C_n^{\mathrm{B,pe}} + C_n^{\mathrm{B,ac}} \quad \text{(A1)}$$

where C_n^{B} is the MWh operating cost for battery n, $C_n^{\mathrm{B,pe}}$ is the price of energy used to charge the battery, $C_n^{\mathrm{B,ac}}$ is the availability cost of battery capacity which can be calculated by:

$$C_n^{\mathrm{B,ac}} = \frac{\text{Replacement Cost}}{E_n^{\mathrm{tc}}} \quad \text{(A2)}$$

where E_n^{tc} is the total lifetime cycling capacity of a battery, which is a function of the depth of discharge $DOD^{\max}$ and the rated life time $LF_n^{\max}$. $E_n^{\sum}$ can be estimated as follows:
Lead acid and lithium-ion battery: See (A3) at the top of the page.

B. Reformulation-Linearization Technique

The mathematical explanation of the linearization procedure is given as follows:

1) Get bilinear term $x_i y_j$, where continuous variables x_i, y_j are all bounded: $x_i^{\min} \leq x_i \leq x_i^{\max}$, $y_j^{\min} \leq y_j \leq y_j^{\max}$.
2) Construct a relaxation: replace each term $x_i y_j$ by an added variable A_{ij}.
3) Adjoin following constraints: See (A4)–(A7) at the top of the page.

The above McCormick's envelopes get an LP relaxation (solvable in polynomial time). Since in our problem, the lower bounds of the variables ($PS_{t,n,u}^{\mathrm{dis}}$, $PS_{t,n,u}^{\mathrm{ch}}$ and $R_{t,i,u}$) are all 0, constraint (A4) can be represented as $A_{ij} \geq 0$.

REFERENCES

[1] M. Gannon, Emerging Rate-of-Change-of-Frequency Problem in the NEM: Best-practice Regulatory Analysis of Options, 2014.

[2] Y. G. Rebours, D. S. Kirschen, M. Trotignon, and S. Rossignol, "A survey of frequency and voltage control ancillary services—Part I: Technical features," *IEEE Trans. Power Syst.*, vol. 22, no. 1, pp. 350–357, Feb. 2007.

[3] R. Doherty *et al.*, "An assessment of the impact of wind generation on system frequency control," *IEEE Trans. Power Syst.*, vol. 25, no. 1, pp. 452–460, Feb. 2010.

[4] F. Fernandez-Bernal, I. Egido, and E. Lobato, "Maximum wind power generation in a power system imposed by system inertia and primary reserve requirements," *Wind Energy*, vol. 18, no. 8, pp. 1501–1514, Aug. 2015.

[5] National Grid Frequency Response Working Group, Frequency Response Technical Sub-Group Report, Nov. 2011, Tech. Rep. [Online]. Available: http://www.nationalgrid.com/NR/rdonlyres/2AFD4C05-E169-4636-BF02-DC67F80F9C2/50090/FRTSGGroupReport_Final.pdf

[6] J. O'Sullivan *et al.*, "Studying the maximum instantaneous nonsynchronous generation in an island system-frequency stability challenges in Ireland," *IEEE Trans. Power Syst.*, vol. 29, no. 6, pp. 2943–2951, Nov. 2014.

[7] N. Wang, Y. Ma, and J. Wang, "Analysis of power system security and stability caused by large-scale wind power grid integration," *Elect. Power Construct.*, vol. 32, no. 11, pp. 77–80, Nov. 2011, in Chinese.

[8] S. Sharma, S. H. Huang, and N. Sarma, "System inertia frequency response estimation and impact of renewable resources in ERCOT interconnection," in *Proc. IEEE PES General Meeting*, 2011, pp. 1–6.

[9] L. Sigrist, "A UFLS scheme for small isolated power systems using rate-of-change of frequency," *IEEE Trans. Power Syst.*, vol. 30, no. 4, pp. 2192–2193, Jul. 2015.

[10] C. B. Somuah and F. C. Schweppe, "Economic dispatch reserve allocation," *IEEE Trans. Power App. Syst.*, vol. PAS-100, no. 5, pp. 2635–2642, May 1981.

[11] J. F. Restrepo and F. D. Galiana, "Unit commitment with primary frequency regulation constraints," *IEEE Trans. Power Syst.*, vol. 20, no. 4, pp. 1836–1842, Nov. 2005.

[12] E. Ela *et al.*, "Market designs for the primary frequency response ancillary service—Part I: Motivation and design," *IEEE Trans. Power Syst.*, vol. 29, no. 1, pp. 421–431, Jan. 2014.

[13] R. Doherty, G. Lalor, and M. O'Malley, "Frequency control in competitive electricity market dispatch," *IEEE Trans. Power Syst.*, vol. 20, no. 3, pp. 1588–1596, Aug. 2005.

[14] H. Ahmadi and H. Ghasemi, "Security-constrained unit commitment with linearized system frequency limit constraints," *IEEE Trans. Power Syst.*, vol. 29, no. 4, pp. 1536–1545, Jul. 2014.

[15] H. Chavez, R. Baldick, and S. Sharma, "Governor rate-constrained OPF for primary frequency control adequacy," *IEEE Trans. Power Syst.*, vol. 29, no. 3, pp. 1473–1480, May 2014.

[16] Y. Y. Lee and R. Baldick, "A frequency-constrained stochastic economic dispatch model," *IEEE Trans. Power Syst.*, vol. 28, no. 3, pp. 2301–2312, Aug. 2013.

[17] F. Teng, V. Trovato, and G. Strbac, "Stochastic scheduling with inertia-dependent fast frequency response requirements," *IEEE Trans. Power Syst.*, to be published.

[18] Y. Wen, C. Guo, D. S. Kirschen, and S. Dong, "Enhanced security-constrained OPF with distributed battery energy storage," *IEEE Trans. Power Syst.*, vol. 30, no. 1, pp. 98–108, Jan. 2015.
[19] A. Oudalov, D. Chartouni, and C. Ohler, "Optimizing a battery energy storage system for primary frequency control," *IEEE Trans. Power Syst.*, vol. 22, no. 3, pp. 1259–1266, Aug. 2007.
[20] E. Hsieh and R. Johnson, "Frequency response from autonomous battery energy storage," in *Proc. CIGRE Grid of the Future Symp.*, 2012, pp. 1–6.
[21] G. Delille, B. Francois, and G. Malarange, "Dynamic frequency control support by energy storage to reduce the impact of wind and solar generation on isolated power system's inertia," *IEEE Trans. Sustain. Energy*, vol. 3, no. 4, pp. 931–939, Oct. 2012.
[22] I. Egido, L. Sigrist, E. Lobato, and L. Rouco, "Energy storage systems for frequency stability enhancement in small-isolated power systems," in *Proc. Int. Conf. Renewable Energies and Power Quality*, 2015, pp. 1–6.
[23] P. Kundur, *Power System Stability and Control*. London, U.K.: McGraw-Hill, 1994.
[24] H. Pandzic, Y. Dvorkin, T. Qiu, Y. Wang, and D. S. Kirschen, "Toward cost-efficient and reliable unit commitment under uncertainty," *IEEE Trans. Power Syst.*, to be published.
[25] T. A. Nguyen and M. L. Crow, "Stochastic optimization of renewable-based microgrid operation incorporating battery operating cost," *IEEE Trans. Power Syst.*, to be published.
[26] Y. Wen, C. Guo, H. Pandzic, and D. S. Kirschen, "Enhanced security constrained unit commitment with emerging utility-scale energy storage," *IEEE Trans. Power Syst.*, vol. 31, no. 1, pp. 652–662, Jan. 2016.
[27] Lithium-Ion Battery Life [Online]. Available: http://www.saftbatteries.com/battery-search/intensium%C2%AE-max
[28] S. Maslennikov and E. Litvinov, "Adaptive emergency transmission rates in power system and market operation," *IEEE Trans. Power Syst.*, vol. 24, no. 2, pp. 923–929, May 2009.
[29] H. D. Sherali and W. P. Adams, *A Reformulation-Linearization Technique for Solving Discrete and Continuous Nonconvex Problems*. Berlin, Germany: Springer, 1998.
[30] Data File for Frequency Dynamics Analysis [Online]. Available: http://www.cee.cqu.edu.cn/Teacherweb_Article.asp?id=1175&tid=1253&y_id=1142

Yunfeng Wen (M'15) received his Ph.D. degree in electrical engineering from Zhejiang University, Hangzhou, China, in 2015. From 2012 to 2013, he was a visiting Ph.D. student with the University of Washington, Seattle, WA, USA.

He is currently a Lecturer in the School of Electrical Engineering at Chongqing University, Chongqing, China.

Wenyuan Li (F'02) is currently a Professor in the School of Electrical Engineering at Chongqing University, Chongqing, China, and an Adjunct Professor with Simon Fraser University, Burnaby, BC, Canada.

Dr. Li is a Fellow of the Canadian Academy of Engineering, Fellow of the Engineering Institute of Canada, and also Academician of the Chinese Academy of Engineering. He was the recipient of several awards, including the IEEE Power Engineering Society Roy Billinton Power System Reliability Award in 2011, the International PMAPS Merit Award in 2012, and the IEEE Canada Power Medal in 2014.

Gang Huang (S'15) is pursuing the Ph.D. degree in the College of Electrical Engineering, Zhejiang University, Hangzhou, China. He is currently a visiting Ph.D. student with the Energy Systems Division, Argonne National Laboratory, Argonne, IL, USA.

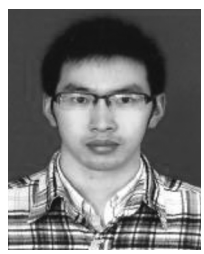

Xuan Liu (M'14) received the B.S. and M.S. degrees from Sichuan University, China, in 2008 and 2011, and Ph.D. degree from Illinois Institute of Technology, USA, in 2015, respectively, all in electrical engineering.